J. Fluid Mech. (2001), *vol.* 448, *pp.* 387–410.
DOI: 10.1017/S0022112001006231 Printed in the United Kingdom

Stability of free-surface thin-film flows over topography

By SERAFIM KALLIADASIS[1] AND G. M. HOMSY[2]†

[1]Department of Chemical Engineering, University of Leeds, Leeds LS2 9JT, UK
[2]Department of Chemical Engineering, Stanford University, Stanford, CA 94305, USA

(Received 15 October 2000 and in revised form 31 May 2001)

We consider the stability of the steady free-surface thin-film flows over topography examined in detail by Kalliadasis *et al.* (2000). For flow over a step-down, their computations revealed that the free surface develops a ridge just before the entrance to the step. Such capillary ridges have also been observed in the contact line motion over a planar substrate, and are a key element of the instability of the driven contact line. In this paper we analyse the linear stability of the ridge with respect to disturbances in the spanwise direction. It is shown that the operator of the linearized system has a continuous spectrum for disturbances with wavenumber less than a critical value above which the spectrum is discrete. Unlike the driven contact line problem where an instability grows into well-defined rivulets, our analysis demonstrates that the ridge is surprisingly stable for a wide range of the pertinent parameters. An energy analysis indicates that the strong stability of the capillary ridge is governed by rearrangement of fluid in the flow direction owing to the net pressure gradient induced by the topography at small wavenumbers and by surface tension at high wavenumbers.

1. Introduction

Flow of thin viscous films over topographical features frequently arises in a large variety of coating applications and is a necessary step in the fabrication of a large number of products and devices. Typical applications include the fabrication of microelectronic components, compact disks and optical devices, and manufacturing of magnetic memory devices and magnetic disks. A common characteristic of these devices is that the substrates are not flat, but exhibit a topography that leads to development of variations in the thickness of the coating.

Theoretical developments in the area include the derivation of a one-dimensional free-surface evolution equation based on the lubrication approximation by Stillwagon & Larson (1998) and Schwartz & Weidner (1995) who also presented an analytical solution to the problem of flow over a curved substrate with a curvature discontinuity. Pritchard, Scott & Tavener (1992) considered the flow of a thin liquid film down an inclined plane with a small slope topography and in the presence of inertia; analytical solutions valid for thin films over large width features and thick films over small width features have been obtained by Stillwagon & Larson (1990). Analytical solutions for thin viscous films over shallow features have also been obtained by Fernandez-Parent, Lammers & Decré (1998) whereas Peurrung & Graves (1993) considered steady flows

† Present address: Department of Mechanical Engineering, University of California at Santa Barbara, Santa Barbara, CA 93106, USA.

over two-dimensional topography. Pozrikidis & Thoroddsen (1991) solved numerically the full Stokes equations for a liquid film flowing down an inclined wall over a particle arrested on the wall and in the limit where the particle size is much smaller than the film thickness. Finally, Kalliadasis, Bielarz & Homsy (2000) performed an extensive parametric study for flow over topography for a wide range of the parameters involved.

Experimental investigations include studies of flow of thin viscous films over one-dimensional trenches by Stillwagon & Larson (1990, 1998) whose experiments clearly show that the free surface is not flat, but exhibits a series of capillary waves, one of which, substantially more pronounced than the rest, we have already referred to as the 'capillary ridge'. Capillary ridges have also been observed in the experiments by Fernandez-Parent *et al.* (1998), Messé & Decré (1997) and Decré, Fernandez-Parent & Lammers (1999). For flow over two-dimensional topographical features, Peurrung & Graves (1993) and Messé & Decré (1997) have observed two-dimensional capillary ridges or 'pile-ups'.

We are interested in flow over sharp edges and steps. For flow over a step-down, Kalliadasis *et al.* (2000) demonstrated that such variations take the form of an asymmetric capillary ridge. The topography will create interfacial curvature and therefore a capillary pressure that will influence the flow features and cause the formation of a capillary ridge just before the entry to the step. Hence, ridge formation is a manifestation of the capillary pressure gradient induced by the substrate curvature and the profile of the free-surface results from the competition between the substrate feature, which creates an interfacial shape that is an impression of the topography, and surface tension which tends to flatten the free surface. The height of the ridge was found to be a strong function of the step depth and step steepness, with the higher ridges appearing for steep substrate features of significant depth.

Much of the motivation for the present study arose from possible connections between this problem and other thin-film problems exhibiting ridges; a capillary ridge is present in the problem of a contact line driven by a body force (Troian *et al.* 1989; Spaid & Homsy 1996; Bertozzi & Brenner 1997) or a temperature gradient (Marangoni effect) over a flat substrate (Cazabat *et al.* 1990). In the moving contact-line problem, the formation of the ridge is due to the response of the free surface to pressure build-up in the vicinity of the contact line as a result of the kinematic requirement that the streamwise velocity gradually decays as the contact point is approached and then reverses as fluid leaves the contact-line region (Goodwin & Homsy 1991). This capillary ridge is known to become unstable to spanwise perturbations and such instabilities have been analysed for contact lines advancing over smooth planar surfaces by a number of authors (Troian *et al.* 1989; Spaid & Homsy 1996; Bertozzi & Brenner 1997; Kondic & Bertozzi 1999; Kalliadasis 2000). The resulting fingering instability has been ultimately linked to the presence of the capillary ridge (Bertozzi & Brenner 1997); we expect a profile without a ridge to be stable. This was shown by Bertozzi & Brenner (1997) for a contact line advancing over an inclined plane with small inclination angle in which case the hydrostatic head associated with the gravitational component normal to the substrate becomes important, suppressing the ridge that would otherwise form. Bertozzi & Brenner showed that profiles without ridges are linearly stable with respect to disturbances in the spanwise direction.

Although there have been both experimental and theoretical studies for flow of thin viscous films over surface features and the type of steady solutions that occur, to date there has not been a study of the stability of these solutions. In this paper,

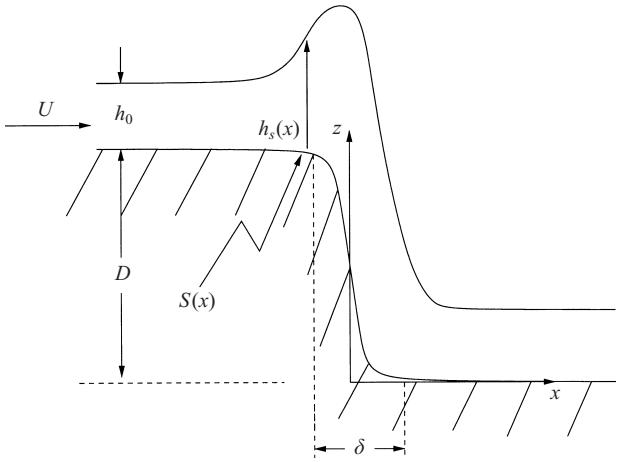

FIGURE 1. Flow over a step-down of depth D and wall steepness δ. The topography is given by $S(x) = D[0.5 - (1/\pi)\tan^{-1}(x/\delta)]$ with respect to an orthogonal coordinate system (x, z) with origin on the step-down. The fluid flows from left to right with a characteristic velocity U and thickness h_0 away from the step. $h_s(x)$ denotes the steady-state deviation height of the free surface with respect to the topography $S(x)$.

we develop a stability theory for free-surface thin-film flows over topography using the flow over a step-down as a model system.

Figure 1 sketches the flow situation in which a thin viscous fluid of viscocity μ, surface tension σ, density ρ and thickness h_0 is flowing over a step of depth D and steepness δ. The fluid flows from left to right driven by a flux Uh_0 due to an external body force with a characteristic velocity U. The basic equation for the evolution of the film height h_s, where the subscript s denotes steady-state, is given by Kalliadasis *et al.* (2000). The equation is based on the lubrication approximation (see Kalliadasis *et al.* for a justification). To balance viscous effects, capillary forces and mean flow, we non-dimensionalize h_s, D and S with h_0, and x and δ with the capillary scale ℓ defined as $\ell = h_0/Ca^{1/3}$ with $Ca = \mu U/\sigma$ the capillary number. The topography shape with respect to the orthogonal coordinate system (x, z) whose origin is placed at the step-down is taken to be

$$S(x) = D\left[\frac{1}{2} - \frac{1}{\pi}\tan^{-1}\left(\frac{x}{\delta}\right)\right]. \tag{1.1}$$

This particular choice for the topography shape approximates a sharp wall in the limit of $\delta \to 0$.

Following Kalliadasis *et al.* (2000), steady-state flows are governed by a modified Landau–Levich equation which includes the topographical forcing as an additional capillary pressure:

$$h_{sxxx} = -S_{xxx} + \frac{1 - h_s^3}{h_s^3}, \tag{1.2a}$$

subject to the boundary conditions

$$h_s(\to \pm\infty) = 1. \tag{1.2b}$$

Solutions of this equation for $\delta = 0.001$ and different step heights are shown in figure 2. In each case, the step is centred at $x = 0$ and falls according to equation (1.1); because of our scaling the surface is one unit below the film far from the step

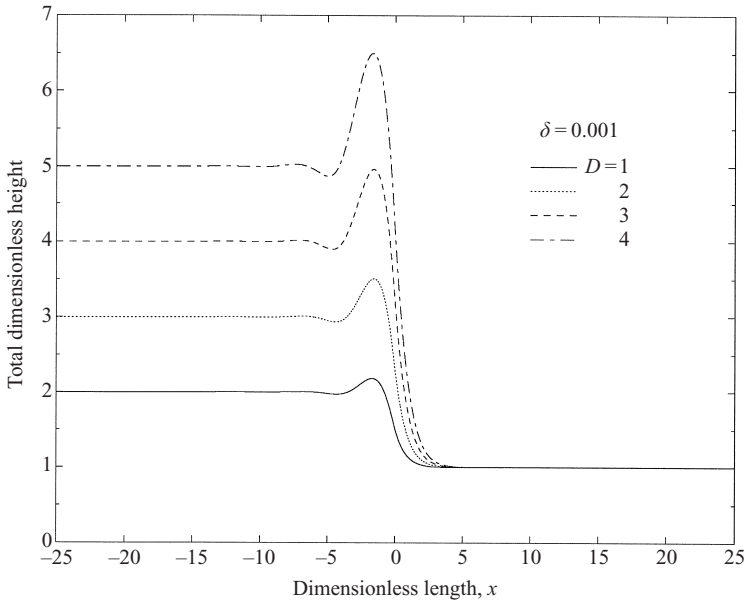

FIGURE 2. Free-surface profile, $h_s(x) + S(x)$ for flow over a step-down for $\delta = 0.001$ and different D values. Note the presence of a capillary ridge just before the entrance to the step whose height increases as D increases.

itself. The feature of interest of these solutions is the presence of a large asymmetric capillary ridge that forms just before the step.

We consider the linear stability of the steady solutions in figure 2 with respect to disturbances in the spanwise direction. There are two main goals to the investigation to be described in the present paper. The first is to construct the spectrum of the linearized operator of the nonlinear system and hence address the issue of stability of the capillary ridge with respect to infinitesimal disturbances in the spanwise direction. The second goal is to infer, from an energy analysis, the physical mechanism responsible for the evolution of infinitesimal disturbances in the spanwise direction and the influence of the topography on the stability characteristics of the capillary ridge.

2. The eigenvalue problem

The starting point for the stability theory is the two-dimensional evolution equation for the free surface which in dimensional variables is:

$$3\mu\frac{\partial h}{\partial t} + \frac{\mu U}{h_0^2}\frac{\partial}{\partial x}(h^3) + \sigma\frac{\partial}{\partial x}[h^3(h_{xxx} + S_{xxx} + h_{yyx})] + \sigma\frac{\partial}{\partial y}[h^3(h_{xxy} + h_{yyy})] = 0, \quad (2.1a)$$

with $h(x, y, t)$ the deviation height and y the spanwise coordinate. Consistent with the lubrication approximation, the mean curvature of the free surface is approximated by $h_{xx} + S_{xx} + h_{yy}$ for a one-dimensional topography shape $S(x)$.

To balance the viscous force, external body force and capillary force in (2.1a), the following non-dimensionalization is introduced,

$$h \to \frac{h}{h_0}, \quad x \to \frac{x}{\ell}, \quad y \to \frac{y}{\ell}, \quad t \to \frac{t}{3\ell/U}, \quad S \to \frac{S}{h_0},$$

where ℓ/U is the convective timescale. Equation (2.1*a*) then becomes:

$$\frac{\partial h}{\partial t}+\frac{\partial}{\partial x}(h^3)+\frac{\partial}{\partial x}[h^3(h_{xxx}+S_{xxx}+h_{yyx})]+\frac{\partial}{\partial y}[h^3(h_{xxy}+h_{yyy})]=0. \tag{2.1b}$$

Let $h(x,y,t)=h_s(x)+\hat{h}(x,y,t), \hat{h}\ll h_s$. Linearizing (2.1*b*) and using the steady-state equation (1.2*a*), we obtain the evolution equation for the disturbance

$$\frac{\partial \hat{h}}{\partial t}+3\frac{\partial}{\partial x}(h_s^2\hat{h})+\frac{\partial}{\partial x}\left[h_s^3(\hat{h}_{xxx}+\hat{h}_{yyx})+3\frac{1-h_s^3}{h_s}\hat{h}\right]+h_s^3(\hat{h}_{xxyy}+\hat{h}_{yyyy})=0. \tag{2.2}$$

We now seek particular solutions of (2.2) in the form of the normal mode

$$\hat{h}(x,y,t)=\mathrm{e}^{\lambda t+\mathrm{i}ky}\psi(x)+\text{c.c.} \tag{2.3}$$

Such solutions are possible since the problem in (2.2) is homogeneous in both t and y. Substitution of (2.3) into (2.2) then yields the infinite-domain eigenvalue problem

$$\mathscr{L}\psi=\lambda\psi, \tag{2.4a}$$

with boundary conditions

$$\psi \quad \text{bounded as} \quad x\to\pm\infty, \tag{2.4b}$$

where the linear differential operator $\mathscr{L}$ is parameterized by the spanwise wavenumber k,

$$\mathscr{L}=-\frac{\partial}{\partial x}\left[h_s^3\left(\frac{\partial^3}{\partial x^3}(\cdot)-k^2\frac{\partial}{\partial x}(\cdot)\right)+3\frac{1-h_s^3}{h_s}(\cdot)\right] -3\frac{\partial}{\partial x}(h_s^2(\cdot))-h_s^3\left(-k^2\frac{\partial^2}{\partial x^2}(\cdot)+k^4(\cdot)\right). \tag{2.5}$$

The boundary conditions in (2.4*b*) allow for eigenfunctions which do not decay to zero, but instead approach bounded oscillations at the infinities. Understanding of the spectrum is difficult without inclusion of its continuous part, and hence we refrain from imposing the usual boundary conditions $\psi\to 0$ as $x\to\pm\infty$. Indeed, we shall demonstrate that such eigenfunctions dominate the spectrum at small wavenumbers. Our stability analysis will also reveal the existence of a critical wavenumber, that depends on both D and δ, at which localized eigenmodes with $\psi\to 0$ as $x\to\pm\infty$ are born out of the eigenfunctions with bounded oscillations at the infinities.

Whether the disturbance $\hat{h}$ grows in time is then determined by the spectrum of $\mathscr{L}$. We note that for the driven contact-line problem on a planar inclined susbtrate, the pertinent eigenvalue problem for $k=0$ has a one-dimensional null space spanned by the eigenfunction associated with the translational invariance of the system in the streamwise direction (Troian *et al.* 1989). This translational invariance manifests itself as a null eigenfunction at $k=0$ corresponding to the eigenvalue $\lambda=0$ (Kalliadasis 2000) and as the system possesses no other symmetry except the translational invariance, the zero eigenvalue is generically simple. In the present case, however, the presence of the topography breaks the translational symmetry and hence $\lambda=0$ is not an eigenvalue for disturbances of infinite wavelength that decay to zero at infinity.

We define and construct the spectrum of $\mathscr{L}$ using the Evans function method, which we found to be a more efficient, accurate and systematic way of constructing the spectrum and locating the eigenvalues than other methods. The method was first introduced by Evans (1972) in his theory on nerve impulse stability in relation to the

Hodgin–Huxley nerve axon equations. Later, the method was further developed by Jones (1984) to study the stability of pulse solutions of the Fitzhugh–Nagumo equations and by Pego & Weinstein (1992, 1994) and Pego, Smereka & Weinstein (1993) to study the stability of solitary wave solutions of a wide range of nonlinear evolution equations including the generalized KdV, Boussinesq and KdV–Burgers equations.

The problem of relating spectral/Evans function properties to linearized and nonlinear stability has been treated in detail recently by Zumbrun and coworkers (see for example Brin 1998; Bertozzi *et al.* 2001; Hoff & Zumbrun 1999; Gardner & Zumbrun 1998). These authors have examined the spectral stability of a large family of viscous shocks including compressive and undercompressive travelling waves in thin-film models with second- and higher-order dispersion–diffusion terms. The Evans function method was also used by Ye & Chang (1999) for the driven contact-line problem down a prewetted inclined plane in order to formulate a spectral theory that quantifies the delayed rivulet instability at small inclination angles.

We shall demonstrate that there are two types of singularity associated with the spectrum of $\mathscr{L}$: discrete eigenvalues and the continuous essential spectrum. The discrete spectrum consists of decaying eigenfunctions with $\psi(\pm\infty) = 0$. These eigenfunctions correspond to disturbances localized at the capillary ridge. The continuous spectrum consists of those eigenfunctions with bounded oscillatory behaviour as $x \to \pm\infty$ and, unlike the discrete spectrum, these can alter the base flow far from the ridge. Such eigenfunctions have also been constructed for the contact-line problem down a prewetted plane by Ye & Chang (1999). In this case, the continuous spectrum captures the dynamic sensitivity of the front to surface heterogeneity. However, the unstable discrete mode scrutinized by the spectral theory of Troian *et al.* (1989) dominates over the continuous spectrum for all wavenumbers in the spanwise direction, whereas for flow over topography, the continuous spectrum will be shown to dominate the evolution of disturbances at small wavenumbers.

The starting point of the Evans function method is to express the eigenvalue problem (2.4*a*) as a dynamical system

$$\frac{\mathrm{d}\boldsymbol{y}}{\mathrm{d}x} = \boldsymbol{A}(x,\lambda)\boldsymbol{y}, \tag{2.6}$$

where $\boldsymbol{y} = (\psi, \psi_x, \psi_{xx}, \psi_{xxx})^t$ and

$$\boldsymbol{A} = \begin{bmatrix} 0 & 1 & 0 & 0 \\ 0 & 0 & 1 & 0 \\ 0 & 0 & 0 & 1 \\ \alpha_0 & \alpha_1 & \alpha_2 & \alpha_3 \end{bmatrix}$$

with

$$\alpha_0 = 3\frac{h_{sx}}{h_s^5} - k^4 - \frac{\lambda}{h_s^3}, \quad \alpha_1 = -\frac{3}{h_s^4} + 3k^2\frac{h_{sx}}{h_s},$$

$$\alpha_2 = 2k^2, \quad \alpha_3 = -3\frac{h_{sx}}{h_s}.$$

Following Swinton & Elgin (1990) we also define an adjoint problem to (2.6) from

$$\frac{\mathrm{d}\boldsymbol{z}}{\mathrm{d}x} = -\boldsymbol{A}^t\boldsymbol{z}, \tag{2.7}$$

and such that

$$\frac{\mathrm{d}}{\mathrm{d}x}(\boldsymbol{z}^t \cdot \boldsymbol{y}) = 0$$

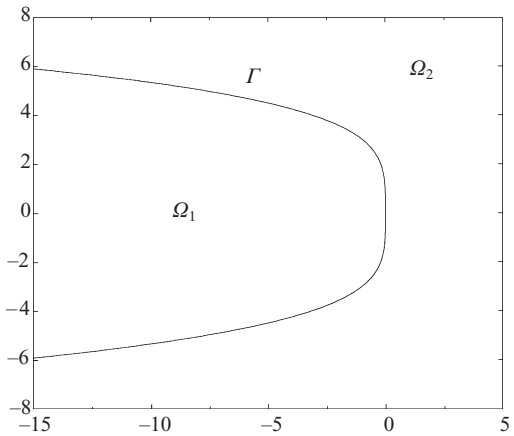

FIGURE 3. Locus of the essential spectrum Γ in the spectral plane (λ_R, λ_I) for $k = 0$. The essential spectrum separates the spectral plane into two regions Ω_1 and Ω_2.

or $\boldsymbol{z}^t \cdot \boldsymbol{y} =$ constant for all x. The behaviour of $\boldsymbol{y}$ and $\boldsymbol{z}$ as $x \to \pm\infty$ is determined by the matrix $\boldsymbol{A}_\infty$ obtained by setting $h_s = 1$ in $\boldsymbol{A}$. The 'spatial' eigenvalues are the eigenvalues of $\boldsymbol{A}_\infty$ determined by the characteristic polynomial

$$\sigma^4 - 2k^2\sigma^2 + 3\sigma + k^4 + \lambda = 0. \tag{2.8}$$

Hence, there are four complex spatial eigenvalues for a given λ in the complex spectral plane. For some specific values of λ, σ is purely imaginary and equal to $\mathrm{i}\alpha$. This is the locus Γ of the essential spectrum and is defined by

$$\Gamma = \{\alpha : \alpha^4 + 2k^2\alpha^2 + 3\mathrm{i}\alpha + k^4 + \lambda = 0, \quad \alpha \in (-\infty, +\infty)\}, \tag{2.9a}$$

which with $\lambda = \lambda_R + \mathrm{i}\lambda_I$ gives

$$\lambda_R = -\tfrac{1}{81}\lambda_I^4 - \tfrac{2}{9}k^2\lambda_I^2 - k^4, \tag{2.9b}$$

and hence, unlike the capillary ridge in Huppert's problem (see Ye & Chang 1999), the essential spectrum in our case is confined to a single curve. A plot of equation (2.9*b*) for $k = 0$ is given in figure 3. The locus Γ of the essential spectrum separates the (λ_R, λ_I) spectral plane into two regions Ω_1 and Ω_2. In Ω_1, three eigenvalues $\sigma_{1,2,3}$ have positive real parts and one eigenvalue σ_4 has a negative real part. In Ω_2, two eigenvalues $\sigma_{1,2}$ have positive real parts and the remaining two eigenvalues $\sigma_{3,4}$ have negative real parts. Hence, $\mathrm{Re}(\sigma_{1,2}) > 0$ and $\mathrm{Re}(\sigma_4) < 0$ for all λ whereas on Γ, one of the eigenvalues is purely imaginary, $\sigma_3 = \mathrm{i}\alpha$, with α the wavenumber parameterizing Γ. Therefore, the spatial eigenvalue σ_3 changes stability as Γ is crossed in the complex λ-plane. This purely imaginary eigenvalue on Γ is responsible for the constant-amplitude oscillations of the eigenfunctions of the essential spectrum as $x \to \pm\infty$.

The behaviour of $\boldsymbol{y}$ and $\boldsymbol{z}$ as $x \to \pm\infty$ is determined by the eigenvectors of $\boldsymbol{A}_\infty$ and $\boldsymbol{A}_\infty^t$ obtained from $\boldsymbol{A}_\infty \boldsymbol{w}_i = \sigma_i \boldsymbol{w}_i$ and $\boldsymbol{A}_\infty^t \boldsymbol{v}_i = \sigma_i \boldsymbol{v}_i$ for $i = 1, 2, 3, 4$ where $\boldsymbol{w}_i$ is an eigenvector of the eigenvalue σ_i of $\boldsymbol{A}_\infty$ and $\boldsymbol{v}_i$ is an eigenvector of $-\sigma_i$ of $-\boldsymbol{A}_\infty^t$, i.e. $\boldsymbol{y}$ and $\boldsymbol{z}$ lie in the stable and unstable manifolds of the systems in (2.6) and (2.7).

For the discrete spectrum, ψ and $\boldsymbol{y}$ must decay to zero as $x \to \pm\infty$. In Ω_1 where $\mathrm{Re}(\sigma_{1,2,3}) > 0$ and $\mathrm{Re}(\sigma_4) < 0$, the behaviour of $\boldsymbol{y}$ as $x \to +\infty$ will be given by

$$\boldsymbol{y}(x \to +\infty) \sim \boldsymbol{w}_4 \exp(\sigma_4 x), \tag{2.10}$$

where $\boldsymbol{A}_\infty \boldsymbol{w}_4 = \sigma_4 \boldsymbol{w}_4$. If we now integrate (2.6) from $+\infty$ along (2.10), the behaviour as $x \to -\infty$ is

$$\boldsymbol{y}(x \to -\infty) \sim \sum_{j=1}^{4} b_{j1}^{-} \boldsymbol{w}_j \exp(\sigma_j x), \tag{2.11}$$

where b_{j1}^{-} are complex coefficients. We obviously want $b_{41}^{-} = 0$. We could then iterate with the complex number λ until b_{41}^{-} vanishes. However, it is often very difficult to integrate $\boldsymbol{y}$ to $-\infty$, or some numerically large number, owing to the exponential growth. Instead, following Swinton & Elgin (1990) we choose to integrate the adjoint problem from $x \to -\infty$:

$$\boldsymbol{z}(x \to -\infty) \sim \boldsymbol{v}_4 \exp(-\sigma_4 x), \tag{2.12}$$

where $\boldsymbol{A}_\infty^t \boldsymbol{v}_4 = \sigma_4 \boldsymbol{v}_4$. We then define, from (2.11) and (2.12), the Evans function $D_1(\lambda)$ in Ω_1 as

$$D_1(\lambda) = \boldsymbol{z}^t(-\infty) \cdot \boldsymbol{y}(-\infty) = b_{41}^{-} \boldsymbol{v}_4^t \cdot \boldsymbol{w}_4 \tag{2.13}$$

after invoking the biorthogonality condition between $\boldsymbol{w}_i$ and $\boldsymbol{v}_j$, $\boldsymbol{v}_j^t \cdot \boldsymbol{w}_i = 0$ for $i \neq j$. Hence, for $b_{41}^{-} = 0$ we must have $D_1(\lambda) = 0$, i.e. the Evans function must vanish. We therefore define the discrete eigenvalues in Ω_1 as the roots of the Evans function (2.13). Alternatively, the Evans function has a zero at λ if, and only if, $\boldsymbol{y}$ and $\boldsymbol{z}$ are homoclinic orbits in systems (2.6) and (2.7). Since now $\boldsymbol{z}^t(-\infty) \cdot \boldsymbol{y}(-\infty) = \boldsymbol{z}^t(x) \cdot \boldsymbol{y}(x) = \text{constant}$, we can integrate (2.6) from $+\infty$ to some point in the neighbourhood of the capillary ridge, say $x = 0$ and the adjoint equation (2.7) from $-\infty$ to the same point and evaluate $D_1(\lambda)$ at that point. This numerical technique, first developed by Swinton & Elgin (1990), removes numerical difficulties at large $\mathbf{y}$ at $+\infty$ and it can be easily formulated in a Newton scheme for seeking the roots of the complex function $D_1(\lambda)$. Alternatively, we can simply scan the complex λ-plane for the roots.

In Ω_2, σ_1 and σ_2 are the spatial eigenvalues with positive real parts and the Evans function must be defined differently. At $+\infty$, the asymptotic behaviour of $\boldsymbol{y}$ is a linear combination of two trajectories

$$\left.\begin{aligned} \boldsymbol{y}_1(x \to +\infty) &\sim \boldsymbol{w}_3 \exp(\sigma_3 x), \\ \boldsymbol{y}_2(x \to +\infty) &\sim \boldsymbol{w}_4 \exp(\sigma_4 x), \end{aligned}\right\} \tag{2.14}$$

such that $\boldsymbol{y}(x \to +\infty) \sim c_1 \boldsymbol{y}_1 + c_2 \boldsymbol{y}_2$. At $-\infty$, the integration of (2.6) using (2.14) as the initial condition yields

$$\left.\begin{aligned} \boldsymbol{y}_1(x \to -\infty) &\sim \sum_{j=1}^{4} b_{j1} \boldsymbol{w}_j \exp(\sigma_j x), \\ \boldsymbol{y}_2(x \to -\infty) &\sim \sum_{j=1}^{4} b_{j2} \boldsymbol{w}_j \exp(\sigma_j x). \end{aligned}\right\} \tag{2.15}$$

To eliminate the undesired growing behaviours $\exp(\sigma_3 x)$ and $\exp(\sigma_4 x)$ we must have

$$\begin{bmatrix} b_{31} & b_{32} \\ b_{41} & b_{42} \end{bmatrix} \begin{bmatrix} c_1 \\ c_2 \end{bmatrix} = \mathbf{0},$$

which has a non-trivial solution for c_1 and c_2 when

$$D_2(\lambda) = \begin{vmatrix} b_{31} & b_{32} \\ b_{41} & b_{42} \end{vmatrix} (\lambda) = 0, \tag{2.16}$$

with $D_2(\lambda)$ the Evans function in Ω_2. However, the shooting scheme from $+\infty$ to

$-\infty$ is again unstable and we must use the adjoint system in (2.7) to formulate an alternative scheme where $D_2(\lambda)$ is evaluated near $x = 0$. In this scheme we integrate the $\boldsymbol{y}$ equation from $+\infty$ along $\boldsymbol{w}_i$ and the $\boldsymbol{z}$ equation from $-\infty$ along $\boldsymbol{v}_j$ to evaluate b_{ji} for $i = 1, 2$ and $j = 3, 4$ and therefore D_2 in (2.16).

The number of discrete eigenvalues within any region in Ω_1 (or Ω_2) can be estimated by using the argument principle of an analytic function

$$n - p = \frac{1}{2\pi \mathrm{i}} \oint_C \frac{D_1'(\lambda)}{D_1(\lambda)} \, \mathrm{d}\lambda = \frac{1}{2\pi} \Delta_C \arg D_1(\lambda), \tag{2.17}$$

where C is a closed contour in Ω_1, n is the number of zeros of $D_1(\lambda)$ and p the number of poles. The right-hand side of (2.17) is the winding number of C', image of C through $D_1(\lambda)$, around the origin. The symbol $\Delta_C \arg$ denotes changes in the argument over the contour C. Following Pego & Weinstein (1992), the Evans function $D_1(\lambda)$ should have no poles in Ω_1 and therefore the number of eigenvalues is solely determined by the winding number of C'. We also used this method to estimate the location of the eigenvalues by shrinking the closed contour successively. This is a very labour-intensive effort and we used (2.17) to determine whether any eigenvalue exists within a certain domain and whether all of them have been located by the shooting scheme.

Construction of the eigenfunctions of the essential spectrum $\psi_\lambda(x)$ can also be obtained from a modified shooting scheme. Since $\mathrm{Re}(\sigma_4) < 0$ and $\sigma_3 = \mathrm{i}\alpha$, the asymptotic behaviour of $\boldsymbol{y}$ as $x \to +\infty$ is a linear combination of two trajectories

$$\boldsymbol{y}(x \to +\infty) \sim c_1 \boldsymbol{y}_1 + c_2 \boldsymbol{y}_2, \tag{2.18}$$

where

$$\boldsymbol{y}_1(x \to +\infty) \sim \boldsymbol{w}_4 \exp(\sigma_4 x),$$

$$\boldsymbol{y}_2(x \to +\infty) \sim \boldsymbol{w}_3 \exp(\mathrm{i}\alpha x).$$

Integrating (2.6) using (2.18) as the initial condition at $+\infty$ yields

$$\boldsymbol{y}(x \to -\infty) \sim c_1 \sum_{j=1}^{4} b_{j1} \boldsymbol{w}_j \exp(\sigma_j x) + c_2 \sum_{j=1}^{4} b_{j2} \boldsymbol{w}_j \exp(\sigma_j x). \tag{2.19}$$

Suppression of the unstable σ_4 mode then requires that

$$c_1 b_{41} + c_2 b_{42} = 0,$$

which gives $c_1 = -c_2 b_{42}/b_{41}$. Hence, with c_2 arbitrary, the transmission coefficient $R(\lambda)$ can be defined as the ratio of the amplitude of oscillations in $\psi_\lambda(x)$ as $x \to +\infty$, c_2, over the amplitude of oscillations as $x \to -\infty$, $c_1 b_{31} + c_2 b_{32}$,

$$R(\lambda) = \frac{b_{41}}{b_{32} b_{41} - b_{42} b_{31}} \equiv \frac{D_1(\lambda)}{D_2(\lambda)}, \tag{2.20}$$

for all λ on Γ. This transmission coefficient is a complex number, in general due to the phase shift in the two oscillations as $x \to \pm\infty$.

We developed a numerical scheme for constructing the spectra of $\mathscr{L}$ using the Evans function shooting approach. The shooting scheme is based on Gear's method with dynamic adjustment of the step-length (Gladwell & Sayers 1980). The scheme also includes projection techniques for removing unwanted growing solutions which are present at either side of the domain. The accuracy of the computations was

$D = 0.5$		$D = 1.0$		$D = 2.0$	
δ	k_c	δ	k_c	δ	k_c
0.1	2.65	0.1	2.67	0.1	2.85
0.01	3.10	0.01	3.37	0.01	2.61
0.005	3.89	0.005	3.60	0.005	2.52

TABLE 1. Critical wavenumber k_c as a function of D and δ.

determined by mesh refinement as well as variation of the integration domain and the point in the neighbourhood of the capillary ridge where the Evans function is evaluated. A different method for the computation of the Evans function based on wedge products of the solution vectors has been developed by Brin (1998) in his study of the stability of viscous shock waves of conservation laws with second-order regularization. Brin also performed winding number computations similar to those reported here.

We finally notice that in the Evans function theory (see for example Gardner & Zumbrun 1998), it is always assumed that the coefficients of the eigenvalue problem decay exponentially to limiting values at the infinities, allowing the application of a certain 'gap lemma' to construct bases of decaying solutions of the eigenvalue problem at $\pm\infty$ in a manner that is analytic in λ and on an open neighbourhood of the resolvent set. This assumption is obviously violated here, as the topographical forcing term decays algebraically. However, as Gardner & Zumbrun (1998) point out in their study of stability of viscous shock fronts with second-order regularization, the assumption of exponential growth is not necessary in the scalar case, for which a 'positive spectral gap' between decaying and growing solutions is maintained even as λ approaches the essential spectrum, thus allowing an analytic continuation of the Evans function into the region of the essential spectrum.

3. Results

3.1. *Structure of the spectrum*

Our calculations revealed that discrete eigenfunctions exist in Ω_2 and only for wavenumbers $k > k_c(D, \delta)$. Figure 4 depicts the dispersion relation for the least stable eigenvalue $\lambda = \lambda(k)$ for $D = 1$ and $\delta = 0.01$. Calculations were performed for several values of D and δ, with no changes in the qualitative nature of the results. In all cases, the least stable eigenvalue is negative and the capillary ridge is therefore stable with respect to infinitesimal disturbances in the spanwise direction.

For wavenumbers less than the critical wavenumber k_c, only the essential spectrum is present. Table 1 gives k_c for different values of D and δ. The corresponding eigenvalue is $-k_c^4$. Notice that for small D, k_c is an increasing function of $1/\delta$; however, for large D values, k_c decreases as $1/\delta$ increases, and thus the region in which only the continuous spectrum is present becomes smaller, but the variation is not large in any case. We also point out that Hoff & Zumbrun (2000) have proved asymptotic stability for scalar viscous shock fronts of conservation laws with second- and higher-order regularization, provided the Evans function has no zeros in Ω_2 (which is the case here for $k < k_c$).

Turning now to the eigenfunctions, figures 5(a) and 5(b) depict the unnormalized discrete modes for $D = 1$, $\delta = 0.1$ and $k = 2.7$, $k = 5$, respectively. Notice the presence

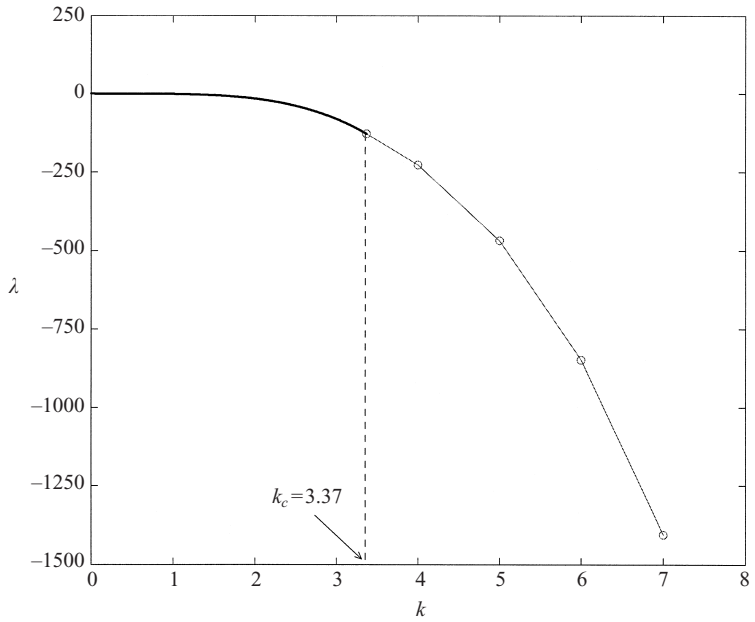

FIGURE 4. Dispersion relation for the eigenvalue λ versus the spanwise wavenumber k for $D = 1$ and $\delta = 0.01$. The critical wavenumber above which discrete modes exist is $k_c = 3.37$. The solid line represents the continuous spectrum for $k \leqslant k_c$ given by $\lambda = -k^4$.

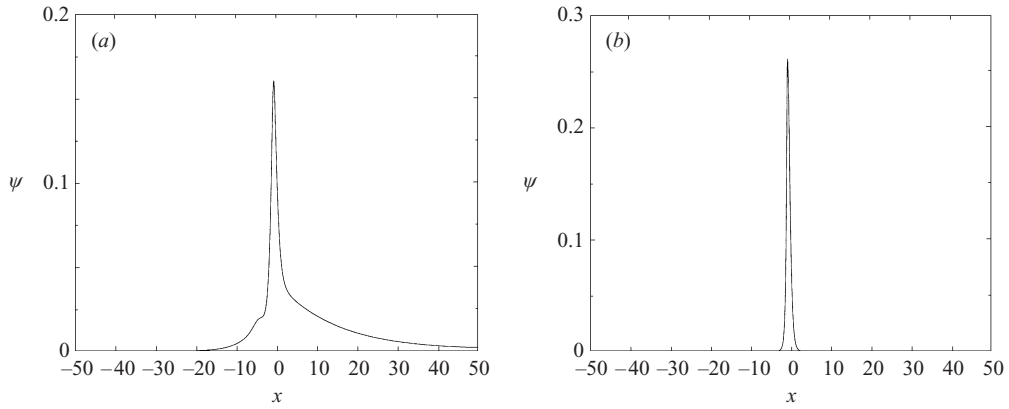

FIGURE 5. (*a*) Discrete eigenfunction for $D = 1$, $\delta = 0.1$ and $k = 2.7$. (*b*) Discrete eigenfunction for $D = 1$, $\delta = 0.1$ and $k = 5$.

of a maximum in the eigenfunctions near $x = 0$. The region of rapid variation for ψ corresponds to the region of rapid variation of the base-state flow and hence the discrete modes are very localized near the capillary ridge. These real modes resemble stationary solitary waves with a characteristic width that decreases as the spanwise wavenumber k increases (see figure 5).

Now consider the continuous spectrum. The solid curve in figure 4 is given by $\lambda = -k^4$ corresponding to $\lambda_I = 0$ in (2.9*b*). This is the point at which the locus of the essential spectrum Γ intersects the λ_R-axis of the spectral plane. We have already pointed out that Γ is parameterized by the wavenumber α of oscillations of the continuous eigenfunctions as $x \to \pm\infty$. As $\alpha \to 0$, the essential modes on Γ

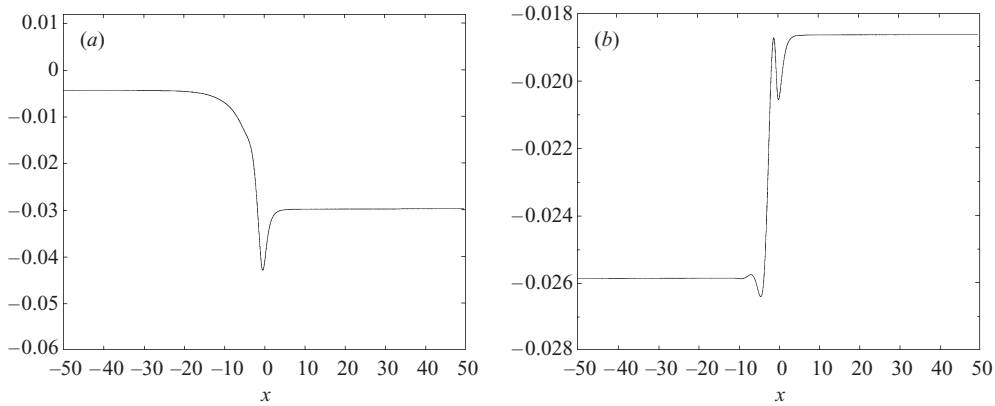

FIGURE 6. Continuous eigenfunction for $\alpha = 0$. (*a*) $D = 0.5$, $\delta = 0.5$, $k = 2.5$; (*b*) $D = 1$, $\delta = 0.1$, $k = 1$.

approach the λ_R-axis and the wavelength of the oscillations becomes infinitely large. All essential modes for $\alpha \neq 0$ are complex except for the limiting eigenfunction at $\alpha = 0$, which is real. This limiting real eigenfunction approaches constants $c_\pm$ as $x \to \pm\infty$, respectively. Figure 6 shows two such modes for $D = 0.5$, $\delta = 0.5$, $k = 2.5$ and $D = 1$, $\delta = 0.1$, $k = 1$. As $k \to k_c^-$, c_- or $c_+ \to 0$ and the discrete mode generated at k_c has the same shape as the continuous mode at this point, but approaches zero very slowly as $x \to +\infty$ or $x \to -\infty$, respectively. When $c_- = 0$, (which is always the case for small D and large δ), the corresponding essential eigenfunction has $R(\lambda) = \infty$. At the same time, $D_2(\lambda) = 0$, consistent with an infinite transmission coefficient, indicating that the discrete mode in Ω_2 and at $k = k_c$ is embedded in the essential spectrum. When $c_+ = 0$, the corresponding essential eigenfunction has a zero transmission coefficient whereas the discrete mode is not embedded in the essential spectrum. As k deviates from k_c, the width of the discrete mode decreases rapidly while both discrete and limiting continuous modes move to the left of the spectral plane with the distance between the two modes increasing as k increases and hence $\lambda(k)$ in figure 4 decays more slowly than $-k^4$. Notice that as with the discrete modes, the region of rapid variation for the continuous modes corresponds to the region of rapid variation of the base-state flow.

Although the locus Γ of the essential spectrum depends only on k (and hence the dispersion relation for $k \leqslant k_c$ is independent of the base-state flow $h_s(x)$), the functional form of the continuous eigenfunctions obviously does depend on $h_s(x)$. Figures 7 and 8 show the continuous (unnormalized) eigenfunctions for two different sets of λ, k, D and δ.

3.2. *Relevance of the continuous spectrum*

The eigenvalues of the linearized system predict the long-time state of the system, strictly speaking, the asymptotic behaviour as $t \to \infty$. The existence of a critical wavenumber k_c above which discrete modes are present indicates that, for $k < k_c$, localized disturbances around the capillary ridge will influence both the ridge and the regions away from it. In this regime, we cannot simply disturb the ridge and expect that the initial disturbance will remain localized around the ridge. Hence, the presence of a continuous spectrum has important implications in the solution of (2.2) as an initial-value problem (see Appendix B for details).

At the same time, the continuous spectrum can be associated with localized dis-

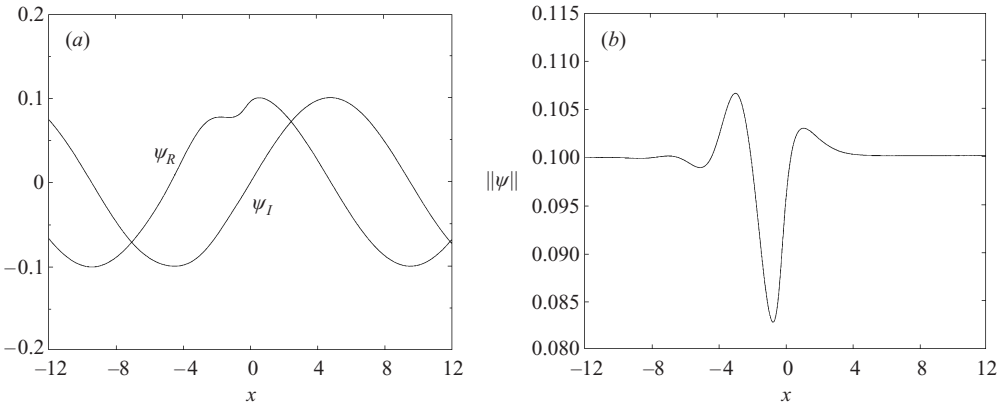

FIGURE 7. (*a*) Continuous eigenfunction for $\lambda_I = -1$, $D = 1$, $\delta = 0.1$ and $k = 0.1$. (*b*) Modulus of the eigenfunction in (*a*).

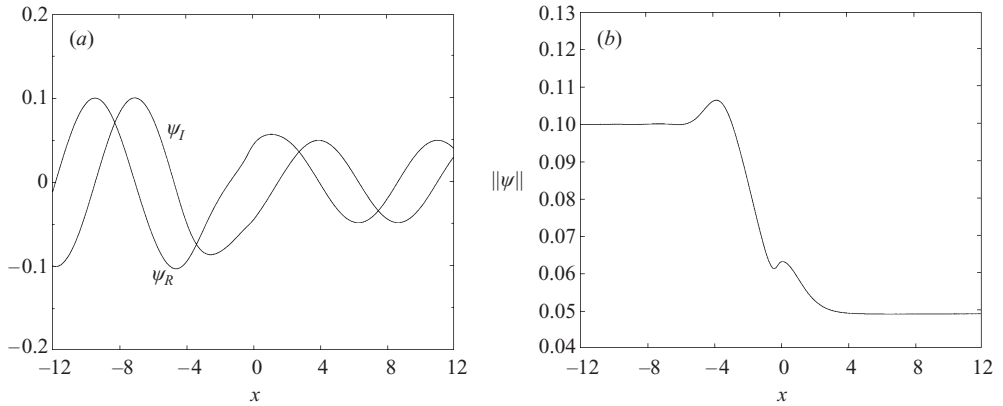

FIGURE 8. (*a*) Continuous eigenfunction for $\lambda_I = -2$, $D = 2$, $\delta = 0.1$ and $k = 1$. (*b*) Modulus of the eigenfunction in (*a*).

turbances on the thin-film regions away from the step. Such localized disturbances, sufficiently far from the capillary ridge, must be expressed in terms of the continuous eigenfunctions which do not decay to zero, but approach bounded oscillations at the infinities – but still within the bounds where the infinite-domain formulation is valid. This is analogous to expansion of finite-mass disturbances with Fourier modes. Such disturbances correspond to step changes in the average interfacial height which generate effective point sources or sinks of liquid. At the same time, as the continuous eigenfunctions do not decay to zero at the infinities, they represent spatially global modes reflecting the response of the base state away from the capillary ridge. However, a detailed consideration of spatial modes and the connection with convective stability theory is beyond the scope of the present paper.

If the base state is a flat film of unit thickness, $\mathscr{L}$ in (2.5) is a differential operator with constant coefficients. Its spectrum then consists of the continuum of Fourier modes $e^{\lambda t + i\alpha x + iky}$ with the dispersion relationship

$$\lambda = -3i\alpha - 2k^2\alpha^2 - \alpha^4 - k^4. \tag{3.1}$$

Since $\lambda_R < 0$, the flat-film regions of thickness 1 are stable. Indeed, as has been shown

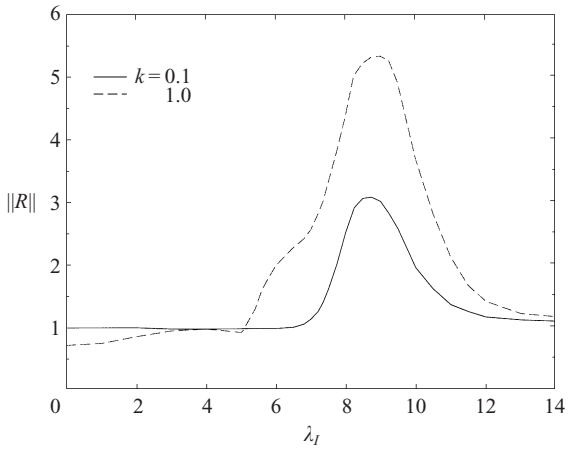

FIGURE 9. Modulus of the transmission coefficient along Γ as a function of λ_I for $D = 1$, $\delta = 0.1$ and two different values of k.

by Benjamin (1957), a thin flat film is always stable and can only be destabilized with small but finite inertia (see also Yih 1963). From the dispersion relation in (3.1) we also obtain $\lambda_I = -3\alpha$. Thus, the normal modes on the flat-film regions represent infinitesimal monochromatic waves that travel steadily with the kinematic wave velocity $-\lambda_I/\alpha = 3$. As λ_I is a linear function of α, the regions $h_s = 1$ away from the capillary ridge are also non-dispersive. Thus, any localized disturbances away from the ridge will not spread, but will propagate at the phase velocity 3 and at the same time decay at the rate λ_R. For the capillary ridge in gravity-driven films, a similar analysis indicates that disturbances on the precursor film have a negative phase velocity and decay very slowly as they travel towards the front. In fact, numerical experiments by Ye & Chang (1999) demonstrated that such disturbances are trapped at the capillary ridge and they are subsequently amplified, whereas in our case, the flow of disturbances on either side of the ridge is in the same direction and hence we anticipate that disturbances can pass from the back to the front of the ridge, leaving it intact.

In any case, the essential spectrum resembles the flat-film Fourier modes away from the capillary ridge, with the constant-amplitude oscillations at the infinities corresponding to the normal modes of the regions $h_s = 1$. In fact, the locus of the essential spectrum Γ defined from (2.9*a*) is described exactly by the flat-film dispersion relationship (3.2.1). The reason is that the ridge decays to such a film at both infinities and the oscillations of the eigenfunctions must also be described by its dispersion relationship. However, the normal modes of the flat film $h_s = 1$ are modified owing to the presence of the capillary ridge (see figures 7 and 8). Finally, the essential eigenfunctions are required to describe disturbances which alter the flow rate and hence the thickness of the film far from the ridge. Any localized disturbance at the flat-film regions and more than a distance of $1/\min|\sigma|$ from the capillary ridge can then be Fourier transformed and its Fourier coefficients must be the coefficients of expansion of the essential modes. The discrete modes also carry mass, as a simple integration of (2.4*a*) indicates: $\int_{-\infty}^{+\infty} \psi \, \mathrm{d}x \neq 0$.

Figure 9 depicts the modulus of the transmission coefficient $||R(\lambda)||$ as a function of λ_I for $D = 1$ and $\delta = 0.1$. The wavenumber α of the oscillations for the essential eigenfunctions as $x \to \pm\infty$ is given by $\alpha = -\frac{1}{3}\lambda_I$. Notice that for $k = 0.1$, $||R|| \simeq 1$ for

a large range of λ_I, indicating that long wavelength disturbances are not influenced by the presence of the capillary ridge. The modulus of the transmission coefficient measures the ratio of the two limiting amplitudes for ψ as $x \to \pm\infty$. Physically, if $||R|| < 1$, sinusoidal waves are dampened as they pass through the capillary ridge from front to back. This transmission coefficient is connected with the phenomenon of radiation transmission through a localized potential well in quantum mechanics as described by the Schrödinger equation (Landau & Lifshitz 1958). In this case, the transmission coefficient is the ratio of the probability density in the transmitted particle to that in the incident particle. However, for the conservative dynamics of the Schrödinger equation, a radiation mode produces both a reflected and a transmitted wave, such that the total energy is conserved. This conservation is lost here owing to the dissipative nature in our system and there is no counterpart to the reflected wave.

In the region $\alpha \to 0$, the eigenfunctions of the essential spectrum approach the constant-amplitude Fourier normal modes of the homogeneous spectrum. These long waves are much longer than the characteristic width of the capillary ridge and hence are oblivious to the presence of the ridge. As a result, $||R||$ is close to unity in this limit and these long-wave modes are hence barely amplified. For transverse wavenumber $k = 0$ (this is essentially the one-dimensional case), the amplification factor $||R||$ approaches unity by conservation of mass (the situation, of course, is different for other problems with a translational symmetry, for example the viscous shock problem studied by Bertozzi *et al.* (2000)). As $\alpha \to \infty$, figure 9 indicates that the transmission coefficient approaches unity as well. This is consistent with the property $D_i(\lambda) \to 1$ as $\lambda \to \infty$ of the Evans functions $D_i(\lambda)$, proved by Pego & Weinstein and other earlier studies. Figure 9 also shows that there exists an intermediate range of $\alpha \sim O(1)$ where $||R||$ exhibits a maximum.

Our calculations indicate that in most cases $||R|| > 1$ (see figure 9). This means that sinusoidal waves are amplified as they pass through the capillary ridge (although for small and large α, radiation amplification is not effective). Hence, for flow over topography, the capillary ridge acts as an amplifier, reminiscent of the driven contact-line problem over a planar substrate where small perturbations in the vicinity of the contact line may cause much larger perturbations to the flow field away from the contact line (Bertozzi & Brenner 1997). Obviously, the amplification observed here is distinctly different from the amplification observed by Bertozzi & Brenner (1997) and more recently Kondic & Bertozzi (1999) for the driven contact-line problem. In this case, there is a strong connection between microscopic-scale perturbations at the precursor film ahead of the apparent contact line, and the transient amplification of these perturbations at the capillary ridge. Bertozzi & Brenner demonstrated that this amplification scales roughly as the inverse precursor film thickness while Kondic & Bertozzi (1999) showed that the amplification factor depends strongly on the width of the imposed perturbation.

We also note that both ψ_R and ψ_I have zero mean as $x \to \pm\infty$. As $\alpha \to 0$, ψ_I approaches zero (with a zero mean) while the wavelength of oscillations for both ψ_R and ψ_I approaches infinity. Hence, for $||R|| \neq 1$ we obtain a limiting eigenfunction $\psi \equiv \psi_R$ that approaches different constants as $x \to \pm\infty$ (see figure 8*b*). In practice, however, the wavenumber α of the continuous spectrum will never be exactly zero as any physical domain is finite. Hence, there is a cutoff for α, α_c. Still, it is the continuous eigenfunctions with small α that dominate the evolution of the disturbances for $k < k_c$.

Finally, we point out that $\mathscr{L}$ is a non-normal operator (not self-adjoint, see Appendix A for details) and the solution of the linearized equations as an initial-value problem might grow by orders of magnitude on a transient time scale, even

though all the eigenvalues are stable. For the driven contact-line problem down an inclined plane, this transient growth effect was suggested by Bertozzi & Brenner (1997) as a means to explain the development of rivulets for small inclination angles. This growth might cause an initially small disturbance to reach a size of order one on a transient time scale, thus exciting nonlinearities and causing an instability. Of course, the degree of non-normality depends on the condition number of the eigenfunctions of $\mathscr{L}$ (Reddy, Schmid & Henningson 1993) and a complete analysis of this effect would involve examination of the resolvent or equivalently the pseudospectrum of $\mathscr{L}$, which is beyond the scope of the present study.

4. Energy analysis

We have found that, unlike the problem of a contact line driven by a body force or a temperature gradient, the capillary ridge for flow over topography is always stable with respect to disturbances in the spanwise direction over the range of parameters $0.5 < D < 5$ and $0.001 < \delta < 0.5$. In addition, for flow over topography there exists a critical wavenumber k_c such that, for $k < k_c$, the least stable eigenfunctions are continuous, whereas for the driven contact-line problem the dominant mode is a discrete eigenfunction.

To explore the mechanism associated with the stability of the capillary ridge, we perform an energy analysis. The method was introduced by Spaid & Homsy (1996) in their work for the driven contact-line problem. Their analysis elucidated the physical mechanism of the instability and demonstrated that the dominant effect is the 'mobility factor', that is, under the action of the body force, thicker films have less resistance than thinner films.

Following Spaid & Homsy (1996), the mechanical energy associated with the disturbance $\hat{h}$ can be defined as

$$E = \frac{1}{2}\int_{-\infty}^{+\infty} \hat{h}\bar{\hat{h}}\,\mathrm{d}x. \tag{4.1a}$$

Taking the inner product of (2.2) with $\hat{h}$ (here we use the usual L^2 inner product $\langle f, g\rangle = \int_{-\infty}^{+\infty} f\bar{g}\,\mathrm{d}x$ for any two functions f and g in L^2), and using the definition of energy, as well as substituting the normal mode (2.3) for $\hat{h}$, gives

$$\frac{\mathrm{d}E}{\mathrm{d}t} = \lambda\langle\psi,\psi\rangle = \langle\mathscr{L}\psi,\psi\rangle. \tag{4.1b}$$

Hence, we can obtain an expression for the rate of energy removal by taking the inner product of the eigenvalue problem with the eigenfunction ψ. The time derivative of the energy can now be normalized so that the total removal energy E^* equals the eigenvalue λ:

$$E^* = \frac{\langle\mathscr{L}\psi,\psi\rangle}{\langle\psi,\psi\rangle} \equiv \lambda. \tag{4.1c}$$

The above definition of energy assumes that ψ is square integrable, i.e. $\int_{-\infty}^{+\infty} ||\psi||^2\,\mathrm{d}x < \infty$. This is definitely the case for the discrete modes of the spectrum where the integral of $||\psi||^2$ converges to a finite value, but not for the continuous eigenfunctions whose energy is infinite. For functions without compact support, such as our continuous modes, the quantity of interest is the energy spectral density per unit length (Champeney 1973). This is computed by taking a long, but finite domain

Term	Functional form	Origin of energy
1	$-3\langle(h_s^2\psi)_x\psi\rangle$	Flow in the x-direction due to the body force
2	$-\langle(h_s^3\psi_{xxx})_x\psi\rangle$	Flow in the x-direction due to the x-curvature
3	$k^2\langle(h_s^3\psi_x)_x\psi\rangle$	Flow in the x-direction due to the y-curvature
4	$-3\langle(h_{sxxx}h_s^2\psi)_x\psi\rangle-$ $-3\langle(S_{xxx}h_s^2\psi)_x\psi\rangle$	Flow in the x-direction driven by the base-state pressure gradient
5	$k^2\langle h_s^3\psi_{xx}\psi\rangle$	Flow in the y-direction due to the x-curvature
6	$-k^4\langle h_s^3\psi^2\rangle$	Flow in the y-direction due to the y-curvature

TABLE 2. Terms comprising the stability problem, along with the physical mechanism associated with each term.

of ψ, computing its energy spectral density, i.e. the energy spectral density of the function that equals ψ in the finite domain but zero everywhere else, and then dividing the resulting quantity by the length of the domain used. (Parseval's theorem in this case states that the integral of the energy spectral density per unit length is equal to the mean square amplitude of ψ (Champeney 1973)). An alternative but equivalent description of the energy is simply the integral of $||\psi||^2$ in a long enough domain $[L_1, L_2]$ divided by the length of the domain $L_2 - L_1$. The integration domain was taken to be $[-30, 30]$ corresponding to $\alpha \simeq 0.1$, and the inner products in (4.1c) are now understood to be finite integrals in the domain $[-30, 30]$.

Having defined the energy for both the discrete and continuous eigenfunctions (obviously, for $k > k_c$, only the energy associated with the discrete modes is relevant), we now turn to equation (4.1c) which contains 6 terms, each of which contributes to the total energy and is associated with a different physical mechanism. Table 2 gives the six terms that comprise $\langle\mathscr{L}\psi, \psi\rangle$ in (4.1c) along with the physical meaning for each term. A sum of all terms in table 2 divided by $\langle\psi^2\rangle$ gives the extended version of (4.1c)

$$\lambda = -3\frac{\langle(h_s^2\psi)_x\psi\rangle}{\langle\psi^2\rangle} - \frac{\langle(h_s^3\psi_{xxx})_x\psi\rangle}{\langle\psi^2\rangle} + k^2\frac{\langle(h_s^3\psi_x)_x\psi\rangle}{\langle\psi^2\rangle}$$
$$-3\frac{\langle[(h_{sxxx} + S_{xxx})h_s^2\psi]_x\psi\rangle}{\langle\psi^2\rangle} + k^2\frac{\langle h_s^3\psi_{xx}\psi\rangle}{\langle\psi^2\rangle} - k^4\frac{\langle h_s^3\psi^2\rangle}{\langle\psi^2\rangle}. \tag{4.2}$$

As our base-flow is stationary, the term associated with flow in the x-direction owing to the reference velocity for the driven contact-line motion studied by Spaid & Homsy (1996) is absent in (4.2). Notice that the terms $\langle(h_{sxxx}h_s^2\psi)_x\psi\rangle$ and $\langle(S_{xxx}h_s^2\psi)_x\psi\rangle$ are lumped together in table 2 as $h_s + S$ is the total free-surface height and it is the sum of the two quantities which represents flow in the x-direction driven by the net base-flow pressure gradient.

The energy calculations were performed for several values of D and δ with no changes in the qualitative nature of the results and hence it is sufficient to discuss the results for the particular choice $D = 1$ and $\delta = 0.1$. Table 3 gives the various contributions to the energy for a wide range of k. As can be seen, for all but the small wavenumbers, the energy is dominated by term 6, which represents damping due to surface tension acting on spanwise curvature. (This same term is responsible for damping of short-wave axial modes in Rayleigh capillary breakup of liquid cylinders.) Term 1, flow in the x-direction owing to the external body force, is always destabilizing, and is the only positive term for all k. In fact, this same term is primarily responsible

https://doi.org/10.1017/S0022112001006231 Published online by Cambridge University Press

k	Term 1	Term 2	Term 3	Term 4	Term 5	Term 6	Total energy
0.00	0.011	-2.918×10^{-3}	0.000	-7.962×10^{-3}	0.000	0.000	0.000
0.25	0.011	-2.740×10^{-3}	-9.307×10^{-5}	-7.930×10^{-3}	-2.900×10^{-4}	-3.976×10^{-3}	-3.906×10^{-3}
0.50	0.013	-2.288×10^{-3}	-3.187×10^{-4}	-7.910×10^{-3}	-9.899×10^{-4}	-6.359×10^{-2}	-6.250×10^{-2}
0.75	0.017	-1.771×10^{-3}	-5.887×10^{-4}	-7.940×10^{-3}	-1.059×10^{-3}	−0.323	−0.316
1.00	0.026	-1.473×10^{-3}	-1.094×10^{-3}	-6.800×10^{-3}	-1.199×10^{-3}	−1.015	−1.000
1.25	0.038	-1.631×10^{-3}	-2.835×10^{-3}	-6.871×10^{-3}	-2.848×10^{-3}	−2.465	−2.441
1.50	0.044	-2.240×10^{-3}	-7.060×10^{-3}	-6.835×10^{-3}	-2.473×10^{-3}	−5.088	−5.063
1.75	0.054	-3.084×10^{-3}	-1.356×10^{-2}	-5.030×10^{-3}	-3.145×10^{-3}	−9.408	−9.379
2.00	0.076	-4.186×10^{-3}	-2.153×10^{-2}	−0.022	-5.971×10^{-3}	−16.022	−16.000
2.25	0.059	-6.508×10^{-3}	-3.225×10^{-2}	−0.0158	-8.348×10^{-3}	−25.626	−25.629
2.50	0.054	-2.031×10^{-2}	-7.048×10^{-2}	−0.012	-6.654×10^{-2}	−38.974	−39.063
3.00	0.071	−1.749	−7.043	−0.182	−0.546	−67.202	−76.652
4.00	0.192	−4.902	−23.456	−0.429	−1.329	−176.619	−206.543
5.00	0.272	−9.843	−50.810	−0.596	−7.370	−376.174	−444.521
6.00	0.327	−16.958	−91.511	−0.715	−20.322	−706.068	−835.247

TABLE 3. Energy results as a function of k for $D = 1$ and $\delta = 0.1$.

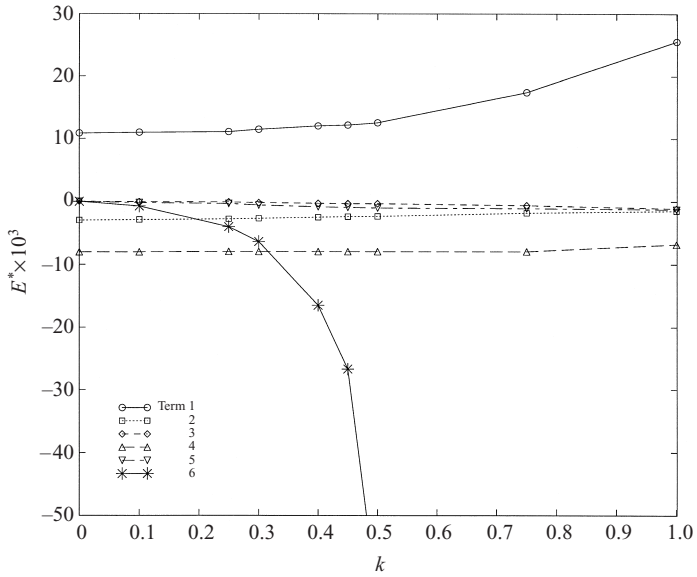

FIGURE 10. Energy results for $D = 1$ and $\delta = 0.1$. The energy is plotted as a function of the spanwise wavenumber k for each of the terms listed in table 2 normalized with $\langle \psi^2 \rangle$. Note that the energy has been multiplied by 10^3.

for the rivulet instability in the driven contact-line problem (Spaid & Homsy 1996). However, as can be seen, it never exceeds term 6, except for small wavenumber. Thus, stability at moderate to large wavenumber is due to surface tension.

We studied the small k regime in more detail, as shown in figure 10. The figure depicts the energy of each term in (4.2) as a function of k for small k. The first feature we note is that, with the exception of terms 1 and 6, most of the contributions to the energy are relatively independent of k. Since term 6 is small for small k, and term 1 is always positive, stability for small k must be due to mechanisms other than spanwise curvature. Most of the negative energy comes from term 4, flow in the x-direction driven by the base-state pressure gradient – the term most directly associated with the topography – with smaller amounts of damping due to term 2, flow in the x-direction due to the x-curvature. As already noted, term 6 is primarily responsible for most of the negative energy in the system for wavenumbers > 0.3. Finally, notice that term 5 (flow in the spanwise direction due to the azimuthal curvature – a destabilizing Rayleigh term for a liquid cylinder) is always negative in contrast to the driven contact-line problem where the same term is always destabilizing.

5. Summary

We have considered the stability of free-surface thin-film flows over topography, the steady states of which have been examined in detail by Kalliadasis *et al.* (2000). For flow over a step-down, the free surface develops a ridge just before the entrance to the step. Such capillary ridges have been observed in the contact-line motion over a planar substrate, and are a key element of the instability of the driven contact line. We were motivated to examine the stability of ridges driven by topography by a possible connection with the driven contact-line problem. We analysed the linear stability of the ridge with respect to disturbances in the spanwise direction. The stability problem

was formulated in a way that allowed for disturbances that did not necessarily decay at the infinities. In this way, we are able to consider the initial-value problem for disturbances and to analyse the complete spectrum. The resulting linear eigenvalue problem proved to be particularly subtle in its structure, necessitating the use of the Evans function method for its numerical solution.

We found that the operator of the linearized system has a continuous spectrum for disturbances with wavenumber less than a critical value; above this value, the spectrum is discrete. The discrete spectrum thus does not exist over the entire range of wavenumbers, but is born from the continuous spectrum at this critical value. The eigenfunctions of the discrete spectrum are localized near the step, whereas those of the continuous spectrum exhibit oscillations of different amplitudes at the infinities. The associated transmission coefficients are computed as a function of the wavenumber of these oscillations. Interestingly, the transmission coefficients are always near or above unity, indicating that the ridge may act as an amplifier for impulses originating at infinity.

Our main result is that, unlike the driven contact-line problem where an instability grows into well-defined rivulets, the topography-driven ridge is surprisingly stable for a wide range of the pertinent parameters. The reasons for the stability of the ridge are established through an energy analysis. Energy is produced or destroyed by the coupling of perturbations with the base flow, and the energy evolution is expressed as a series of mathematical terms, each of which has a specific physical interpretation. The only term found to represent energy production is the same as the one responsible for the rivulet instability, i.e. the flow in the streamwise direction driven by a body force. This term is dominated by other, negative terms, representing energy damping. The mechanism responsible for the damping is found to depend on wavenumber. For small wavenumber, stability is due to rearrangement of fluid in the flow direction owing to the net pressure gradient induced by the topography, whereas for moderate to large wavenumber, stability is due to surface tension acting in concert with spanwise curvature.

S. K. thanks the Chemical Engineering Department at Stanford University for hospitality during a mini-sabbatical visit and the Engineering and Physical Sciences Research Council of England for financial support. G. M. H. acknowledges financial support from the Basic Energy Sciences, US Department of Energy, through grant no. DE-FG03-87ER13673. Thanks also to Kevin Zumbrun for helpful comments and suggestions.

Appendix A. The adjoint eigenvalue problem

The operator $\mathscr{L}$ in (2.4*a*) is non-normal with respect to the usual $L^2(-\infty,+\infty)$ inner product $\langle f,g\rangle = \int_{-\infty}^{+\infty} f\bar{g}\,\mathrm{d}x$ (the overbar designates complex conjugation) for any two functions f and g with appropriate boundary conditions at infinity. The adjoint is defined from

$$\langle \mathscr{L}\psi,\hat{\psi}\rangle = \langle \psi,\mathscr{L}^*\hat{\psi}\rangle + B(\psi,\hat{\psi})|_{-\infty}^{+\infty},$$

where ψ is an eigenfunction of $\mathscr{L}$, $\hat{\psi}$ the adjoint eigenfunction of $\mathscr{L}^*$, and B a bilinear function of ψ, $\hat{\psi}$ and their derivatives representing the boundary terms originating from integrations by parts. To eliminate the boundary terms and define $\mathscr{L}^*$, we are first restricted to the discrete spectrum with exponentially decaying ψ at the infinities. At the same time, since ψ and all its derivatives vanish at the infinities for the discrete

spectrum, the adjoint eigenfunction $\hat{\psi}$ is not required to decay at the infinities so long it does not blow up faster than ψ. With these restrictions, $\langle \mathscr{L}\psi, \hat{\psi}\rangle = \langle \psi, \mathscr{L}^*\hat{\psi}\rangle$ from which the adjoint operator can be easily obtained. We find that $\mathscr{L}$ does not commute with its adjoint $\mathscr{L}^*$ and hence the eigenvalues λ can be complex – the essential spectrum is indeed complex. To define the adjoint operator for the essential modes, the boundary terms $B(\psi, \hat{\psi})$ vanish if the behaviour of the adjoint eigenfunctions is given by $\hat{\psi} \sim \hat{c}_{\pm} e^{i\alpha x}$ as $x \to \pm\infty$ with $\hat{c}_+/\hat{c}_- = c_-/c_+$ where $\psi \sim c_{\pm} e^{i\alpha x}$ as $x \to \pm\infty$, that is, the transmission coefficient for the adjoint continuous eigenfunctions is the inverse of the transmission coefficient of the continuous eigenfunctions of $\mathscr{L}$.

For a discrete spectrum, an arbitrary function Ψ can be represented in the form of a series

$$\Psi = \sum_n \beta_n \psi_n \tag{A 1}$$

where the summation extends over all n, ψ_n are the discrete eigenfunctions and β_n are some constant coefficients. The expansion in (A 1) assumes that the set of eigenfunctions $\{\psi_n\}$ is complete. As the eigenfunctions are known within a multiplicative constant, they can be easily normalized such that their maximum attains a given value. Alternatively, the discrete eigenmodes can be normalized such that $\langle \psi_i, \hat{\psi}_j\rangle = \delta_{ij}$ which for self-adjoint operators is simply $\int_{-\infty}^{+\infty} ||\psi||^2 \, dx = 1$ (in quantum mechanics, this is equivalent to requiring that the sum of all probabilities expressed by the wave function ψ equals unity (Landau & Lifshitz 1958)).

Let us now denote ψ_λ, the eigenfunction corresponding to the eigenvalue λ of the continuous spectrum. In this case, the series in (A 1) is replaced with an integral (much as a Fourier series gives way to a Fourier integral for a periodic function with an infinite period):

$$\Psi = \int_\Gamma \beta_\lambda \psi_\lambda \, d\lambda \tag{A 2}$$

where the integration takes place over all possible values of λ.

The coefficients in (A 1) can be evaluated by using the adjoint eigenfunctions $\hat{\psi}_k$

$$\beta_k = \langle \Psi, \hat{\psi}_k \rangle.$$

To directly generalize this relation to the case of continuous spectrum, the coefficients in (A 2) should be given by

$$\beta_\lambda = \langle \Psi, \hat{\psi}_\lambda \rangle \tag{A 3}$$

with $\hat{\psi}_\lambda$ the adjoint eigenfunction at λ. Combining (A 2) and (A 3) shows that the normalization of the continuous spectrum should be

$$\langle \psi_{\lambda'}, \hat{\psi}_\lambda \rangle = \delta(\lambda' - \lambda), \tag{A 4}$$

with δ the Dirac delta function. Hence, normalizing the continuous eigenfunctions is more involved than the case of the discrete spectrum. For self-adjoint operators, for instance, the requirement that the integral of the squared modulus of the function should be equal to unity cannot be satisfied for the continuous spectrum. In this case, the normalization condition is $\int ||\beta_\lambda||^2 \, d\lambda = 1$. In quantum mechanics (Landau & Lifshitz 1958), this is equivalent to normalizing the functions ψ_λ in such a way that $||\beta_\lambda||^2 \, d\lambda$ is the probability that the physical quantity concerned, in the state described by the wave function Ψ, has a value between λ and $\lambda + d\lambda$. Since the sum of the probabilities of all possible values of λ must be equal to unity, we have $\int ||\beta_\lambda||^2 \, d\lambda = 1$.

Appendix B. The initial-value problem for disturbances

The translational invariance of (2.2) in the spanwise direction allows us to make use of a Fourier transform in y. Because of the linearity of (2.2), the dynamics of each Fourier mode is decoupled. The equation for the disturbance H can then be written as

$$\frac{\partial H}{\partial t} = \mathscr{L}H \quad \text{where} \quad t = 0, \quad H = H_0(x), \tag{B 1}$$

with

$$\lim_{x \to \pm\infty} H_0(x) = 0,$$

where $\mathscr{L}$ is the operator defined in (2.5) and the initial condition is localized around the capillary ridge. Following Huerre (1987), the initial-value problem in (B 1) is equivalent to the impulse response problem

$$\left(\frac{\partial}{\partial t} - \mathscr{L}\right) H = F(x,t),$$

where

$$F(x,t) = H_0(x)\delta(t)$$

is a prescribed forcing function initiated at $t = 0$. As this function cannot produce any effect prior to its application, both the perturbation field H and F must remain zero for $t < 0$: $H(x,t) = F(x,t) = 0$ for $t < 0$. Hence, the impulsive 'force' $F(x)$ is applied in the entire physical domain at time $t = 0$.

We can now apply a Laplace tranform on (B 1), $\tilde{H}(x,s) = \int_0^\infty \mathrm{e}^{-st} H(x,t)\,\mathrm{d}t$, to obtain

$$(s - \mathscr{L})\tilde{H} = H_0, \quad \tilde{H}(x \to \pm\infty) = 0, \tag{B 2}$$

which can be inverted with the introduction of a Green's function $G(x;\xi,s)$

$$\tilde{H} = \int_{-\infty}^{+\infty} G(x;\xi,s) H_0(\xi)\,\mathrm{d}\xi, \tag{B 3}$$

where

$$(s - \mathscr{L})G(x;\xi,s) = \delta(x - \xi). \tag{B 4}$$

Inverting (B 3), we obtain the evolution of the disturbance

$$\begin{aligned} H &= \frac{1}{2\pi\mathrm{i}} \int_{\gamma-\mathrm{i}\infty}^{\gamma+\mathrm{i}\infty} \tilde{H}(x,s)\mathrm{e}^{st}\,\mathrm{d}s \\ &= \frac{1}{2\pi\mathrm{i}} \int_{\gamma-\mathrm{i}\infty}^{\gamma+\mathrm{i}\infty} \int_{-\infty}^{+\infty} G(x;\xi,s) H_0(\xi)\,\mathrm{d}\xi\,\mathrm{d}s, \end{aligned} \tag{B 5}$$

where γ is chosen such that the path integral lies to the right-hand side of all singularities for causality reasons. There are two types of singularities associated with $\mathscr{L}$ (§ 3), the discrete eigenvalues and the continuous essential spectrum. Deforming the path integral in (B 5) appropriately and applying the residue theorem, we obtain

$$H(x,t) = \beta_0 \psi_0(x)\mathrm{e}^{\lambda_0 t} + \int_\Gamma \beta_\lambda \psi_\lambda(x)\mathrm{e}^{\lambda t}\,\mathrm{d}\lambda, \tag{B 6}$$

as the complete set of functions is formed by combining the eigenfunctions of both spectra, with $\{\psi_0, \lambda_0\}$ the discrete mode. Finally, we notice that the expansion

coefficients of the discrete and continuous eigenfunctions can be evaluated by taking the appropriate inner products with the adjoint dicrete and continuous eigenfunctions. However, their exact values are not important as long as $H_0(x)$ is sufficiently rich such that the pertinent β_λ is not zero. Note also that while $\psi(x;\lambda)$ is not localized, $H(x,t)$ must be localized as required by functions which can be Fourier transformed. In essence, the Fourier transform is replaced by an expansion in terms of the continuous eigenfunctions.

REFERENCES

Benjamin, T. B. 1957 Wave formation in laminar flow down an inclined plane. *J. Fluid Mech.* **2**, 554–574.

Bertozzi, A. L. & Brenner, M. P. 1997 Linear stability and transient growth in driven contact lines. *Phys. Fluids* **9**, 530–539.

Bertozzi, A. L., Münch, A., Shearer, M. & Zumbrun, K. 2001 Stability of compressive and undercompressive thin film travelling waves. *Eur. J. Appl. Maths* **12**, 253–291.

Brin, L. Q. 1998 Numerical testing of the stability of viscous shock waves. PhD dissertation, Indiana University.

Cazabat, A. M., Heslot, F., Troian, S. M. & Carles, P. 1990 Fingering instability of thin spreading films driven by temperature gradients. *Nature* **346**, 824–826.

Champeney, D. C. 1973 *Fourier Transforms and their Physical Applications*. Academic.

Decré, M. M. J., Fernandez-Parent, C. & Lammers, J. H. 1999 Flow of a gravity driven thin liquid film over one-dimensional topographies: a tripartite approach. *Proc. 3rd European Coating Symposium* (ed. F. Durst & H. Raszillier). Erlangen.

Evans, J. W. 1972 Nerve axon equations: 1 Linear approximations. *Indiana Univ. Math. J.* **21**, 877–885.

Evans, J. W. & Feroe, J. 1977 Local stability theory of the nerve impulse. *Math. Biosci.* **37**, 23–50.

Fernandez-Parent, C., Lammers, J. H. & Decré, M. M. J. 1998 Flow of a gravity driven thin liquid film over one-dimensional topographies. Philips Research Unclassified Report UR 823/28.

Gardner, R. A. & Zumbrun, K. 1998 The gap lemma and geometric criteria for instability of viscous shock profiles. *Commun. Pure Appl. Maths* **7**, 797–855.

Gladwell, I. & Sayers, D. K. (Eds.) 1980 *Computational Techniques for Ordinary Differential Equations*. Academic.

Goodwin, R. & Homsy, G. M. 1991 Viscous flow down a slope in the vicinity of a contact line. *Phys. Fluids* **3**, 515–528.

Hoff, D. & Zumbrun, K. 2000 Asymptotic behaviour of multidimensional scalar viscous shock fronts. *Indiana Univ. Math. J.* **49**, 427–474.

Huerre, P. 1987 Hydrodynamic instabilities in open flows. *Propagation in Systems Far From Equilibrium* (ed. J. E. Wesfreid, H. R. Brand, P. Manneville, G. Albinet & N. Boccara). Springer.

Jones, C. K. R. T. 1984 Stability of the travelling wave solution of the Fitzhugh–Nagumo system. *Trans. Am. Math. Soc.* **286**, 431–469.

Kalliadasis, S. 2000 Nonlinear instability of a contact line driven by gravity. *J. Fluid Mech.* **413**, 355–378.

Kalliadasis, S., Bielarz, C. & Homsy, G. M. 2000 Steady free-surface thin film flows over topography. *Phys. Fluids* **12**, 1889–1898.

Kondic, L. & Bertozzi, A. L. 1999 Nonlinear dynamics and transient growth of driven contact lines. *Phys. Fluids* **11**, 3560–3562.

Landau, L. D. & Lifshitz, E. M. 1958 *Quantum Mechanics*. Pergamon.

Messé, S. & Decré, M. M. J. 1997 Experimental study of a gravity driven water film flowing down inclined plates with different patterns. Philips Research Unclassified Report NL–UR 030/97.

Pego, R. L., Smereka, P. & Weinstein, M. I. 1993 Oscillatory instability of traveling waves for a KdV–Burgers equation. *Physica* D **67**, 45–65.

Pego, R. L. & Weinstein, M. I. 1992 Eigenvalues and instabilities of solitary waves. *Phil. Trans. R. Soc. Lond.* A **340**, 47–94.

Pego, R. L. & Weinstein, M. I. 1994 Asymptotic stability of solitary waves. *Commun. Math. Phys.* **164**, 305–349.

Peurrung, L. M. & Graves, D. B. 1993 Spin coating over topography. *IEEE Trans. Semicond. Manufact*. **6**, 72–76.

Pozrikidis, C. & Thoroddsen, S. T. 1991 The deformation of a liquid film flowing down an inclined plane over a small particle arrested on the wall. *Phys. Fluids* **3**, 2546–2558.

Pritchard, W. G., Scott, L. R. & Tavener, S. J. 1992 Numerical and asymptotic methods for certain viscous free-surface flows. *Phil. Trans. R. Soc. Lond*. A **340**, 1–45.

Reddy, S. C., Schmid, P. J. & Henningson, D. S. 1993 Pseudospectra of the Orr–Sommerfeld operator. *SIAM J. Appl. Maths* **53**, 15–47.

Schwartz, L. W. & Weidner, D. E. 1995 Modeling of coating flows on curved surfaces. *J. Engng Maths* **29**, 91–103.

Spaid, M. A. & Homsy, G. M. 1996 Stability of Newtonian and viscoelastic dynamic contact lines. *Phys. Fluids* **8**, 460–478.

Stillwagon, L. E. & Larson, R. G. 1990 Leveling of thin films over uneven substrates during spoin coating. *Phys. Fluids* **2**, 1937–1944.

Stillwagon, L. E. & Larson, R. G. 1998 Fundamentals of topographic substrate leveling. *J. Appl. Phys.* **63**, 5251–5258.

Swinton, J. & Elgin, J. 1990 Stability of travelling pulse solutions to a Laser equation. *Phys. Lett*. A **145**, 428–433.

Troian, S., Herbolzheimer, E., Safran, S. & Joanny, J. 1989 Fingering instabilities of driven spreading films. *Europhys. Lett*. **10**, 25–30.

Ye, Y. & Chang, H.-C. 1999 A spectral theory for fingering on a prewetted plane. *Phys. Fluids* **11**, 2494–2515.

Yih, C. S. 1963 Stability of liquid flow down an inclined plane. *Phys. Fluids* **6**, 321–330.